# $^{239}$Pu($n$, $2n$) $^{238}$Pu cross section measurement using a recoil method

Vincent Méot,[1,2,*] Olivier Roig,[1,2] Benoit Laurent,[1,2] Pascal Morel,[1] Jean Aupiais,[1] Olivier Delaune,[1] Gérard Haouat,[1] and Olivier Bouland[3]

[1]*CEA, DAM, DIF, F-91297 Arpajon, France*

[2]*Université de Paris-Saclay, CEA, LMCE, 91680 Bruyères-le-Châtel, France*

[3]*CEA, DES, IRESNE, DER, SPRC, Physics Studies Laboratory, Cadarache, F-13108 Saint-Paul-lez-Durance, France*

(Received 9 November 2020; revised 13 January 2021; accepted 12 April 2021; published 18 May 2021)

A new measurement of the $^{239}$Pu($n$, $2n$) $^{238}$Pu cross section was performed at 7.1, 7.7, and 9.3-MeV incident neutron energy using an activation technique to help resolve inconsistencies in the existing database above the threshold of the reaction. The method is based on the collection of $^{238}$Pu nuclei produced in the ($n$, $2n$) reaction. Although never used before to obtain a neutron cross section, this recoil technics overcomes the difficulty of having deposits of $^{239}$Pu of extremely high purity. The collection efficiency must be determined using previously published data at higher energy, and our measurements are relative to these points. The neutrons were produced via the $^{2}$H($d$, $n$) $^{3}$He reaction. The incident neutron flux was determined via the $^{27}$Al($n$,$\alpha$) $^{24}$Na standard reaction. The present measurements are consistent with the previous data and disagree with the JEFF3.3 evaluation.

DOI: 10.1103/PhysRevC.103.054609

## I. INTRODUCTION

Although neutron-induced threshold reactions are interesting for basic science because they involve the onset of a physical process (neutron emission, fission process, etc., …) these reactions are generally used to determine the fast component of a neutron flux [1,2]. On the other hand, the knowledge of these neutron-induced threshold reactions may be important in the context of the inventory of nuclear waste management [3,4]. For instance, in a nuclear reactor the short-lived $^{238}$Pu ($t_{1/2} = 87.7$yr) nucleus is produced by the ($n$, $2n$) reaction on $^{239}$Pu or by successive neutron captures on the uranium isotopes 235 or 238, followed by $\beta^-$ decays or/and $\alpha$ decays [5]. An accurate evaluation of the $^{238}$Pu production in a fission spectrum is required to estimate the activation and the decay heat of the used nuclear fuel.

If the $^{239}$Pu($n$, $2n$) $^{238}$Pu cross section is relatively well known between 8 and 12 MeV, several models and experimental data disagree in the region between 6 and 8 MeV close to the threshold of the reaction. Figure 1 shows three experimental data sets.

The first published measurements are those of Fréhaut *et al.* [6]. They are based on a high-efficiency $4\pi$ neutron detector. The main drawback of this paper is the poor signal-to-background ratio at the threshold of the reaction ($E_{\text{thres}} =$ 5.67 MeV) since the fission process in this area is 10–100 times more intense than the ($n$, $2n$) reaction. Indeed, these pioneering and noteworthy data suffer from large uncertainties inherent to the employed method.

Another measurement, which can be considered as a reference to date, is that of Lougheed *et al.* [7], performed at 14 MeV. It was performed in the 1970s and reanalyzed and published 25 yr later. This is a $^{239}$Pu activation measurement for which uncertainties are extremely low. A plutonium target with an excellent isotopic ratio ($^{238}$Pu / $^{239}$Pu $\approx 10^{-11}$), and a very high flux neutron irradiation made it possible to produce substantially more $^{238}$Pu nuclei than those initially present in the sample. However, the experimental facility they used for this paper did not enable to measure anywhere other than the 14-MeV region.

The third set of measurements in Fig. 1 is that of Becker and co-workers [8–10] performed with an experimental method consisting in extracting the cross section from the $^{239}$Pu($n$,$2n\gamma$) $^{238}$Pu reaction. To obtain this cross section, it is then necessary to know how each excited level of $^{238}$Pu is populated by the ($n$, $2n$) reaction on $^{239}$Pu. That requires the use of a nuclear reaction model that may generate uncertainties difficult to quantify.

The $^{239}$Pu($n$, $2n$) cross section inferred by Becker and coworkers from this technique exhibits a sudden drop below 8 MeV (Fig. 1). This is also observed in the data of Fréhaut *et al.* [6], which have, however, larger associated uncertainties. In the ($n$,$2n\gamma$) data, it is unclear whether this effect is due to a bias in the model or not. Indeed, at lower excitation energy, i.e., just above the threshold, nuclear structure effects may play a significant role, and some transitions cannot be obtained by a statistical model as is performed in the GNASH code [11] used by the authors in their ($n$,$2n\gamma$) analysis. In Ref. [10] the authors compare the ($n$, $2n$) cross sections obtained using two separate statistical codes, GNASH and IDA [12]. In the 6–8-MeV area, the IDA result is up to 30% higher than the GNASH code resulting in a softer increase in the cross section. More recently, Dupuis *et al.* calculated the $^{239}$Pu($n$, $2n$) cross section within a microscopic approach [13]. Using a JLM folding model [14,15] to describe the neutron-nucleus interaction and with QRPA nuclear-structure ingredients [16], they could not

*Corresponding author: vincent.meot@cea.fr

 

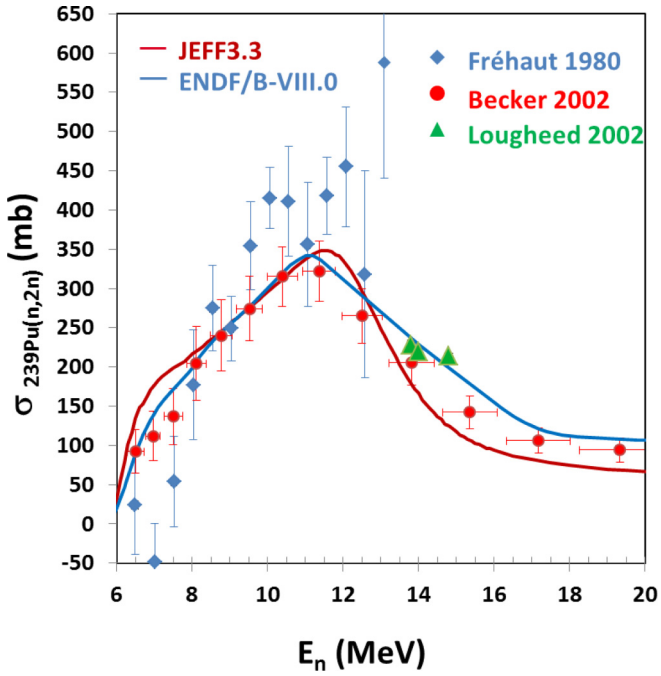


FIG. 1. Evaluations (continuous lines) and experimental measurements (data points) of the $^{239}$Pu$(n, 2n)$ reaction cross section.

explain the $(n, 2n)$ cross-section behavior in the 6–8-MeV energy region.

The evaluation of the $^{239}$Pu$(n, 2n)\,^{238}$Pu cross section just above the threshold of the reaction is problematic because of the opening of the second chance fission channel (fission after the emission of one neutron). Using the so-called "full-model" methodology, such as that carried out in JEFF-3.3 evaluation of the plutonium isotopes [17–19], we know that the shape of the $(n, 2n)$ cross section just above threshold is strongly dependent on the modeling of the second chance fission. As for the $^{239}$Pu cross section the $(n, f)$ channel is much larger than that for the $(n, 2n)$ channel, a small variation in the fission values can have a significant impact on the $(n, 2n)$ cross section. Figure 1 shows noticeable discrepancies at the reaction threshold among recent data evaluations. Note that the ENDF/B VIII.0 $(n, 2n)$ file [20] is based on a least-squares analysis of the experimental data of Becker *et al.* [8] and Lougheed *et al.* [7].

Finally, we must mentioned the integral experiment PROFIL [21], carried out with the PHENIX fast neutron spectrum reactor, which yielded $(n, 2n)$ results, obtained from the analysis of integral measurements. In their work, using the JEFF-3.1 evaluation data set library, the authors obtained a value of 0.793(34) for the calculation/experiment ratio for the integral $^{239}$Pu$(n, 2n)$ cross section. In the 6–8-MeV energy region the JEFF3.1 $^{239}$Pu$(n, 2n)$ cross section is only 6% higher than the JEFF3.3 cross section and a discrepancy with the integral measurement should be observed for this library as well. This result, inconsistent with previous measurements, further confuses our understanding of the cross section in the threshold region. This could be explained: The integral calculation of the $^{239}$Pu$(n, 2n)$ cross section is highly sensitive to the slope of the neutron spectrum in the high-energy tail (5–10 MeV).

Among the $^{239}$Pu$(n, 2n)\,^{238}$Pu measurement methods presented above, the one used by Lougheed *et al.* [7], which consists of a $^{239}$Pu massive sample irradiation followed by a $^{238}$Pu activation measurement, seems to be most interesting because it gives data with very small uncertainties. However, this method requires a plutonium sample enough depleted in $^{238}$Pu to produce significantly more $^{238}$Pu nuclei than those already present in the target before irradiation. Nowadays, it is very difficult to obtain such a pure $^{239}$Pu sample. Therefore, in order to overcome this puzzling problem, we designed and developed an experimental setup which relies on a recoil technique described below, for counting the $^{238}$Pu nuclei produced only by the $(n, 2n)$ reaction. We believe this measurement technique, is capable of yielding good quality data which would help improving the description of the $^{239}$Pu$(n, 2n)\,^{238}$Pu cross section at the threshold and would help also checking for consistency between data and evaluations.

For this purpose, a series of irradiation measurements were undertaken on two actinide nuclei: $^{238}$U and $^{239}$Pu with the high-flux fast-neutron facilities of the CEA-DAM Ile de France. These are presented below and commented on as follows. Section II presents the experimental setup for $(n, 2n)$ cross-section measurements, including the high-flux neutron production, the recoil technique and its utilization, the manufacturing of the actinide deposits, the target assembly with the reaction chamber, the incident neutron monitoring and the recoiling nuclei counting. Our first experiment, presented in Sec. III, was devoted to the study of the $^{238}$U$(n, 2n)\,^{237}$U reaction; it was intended to refine the $(n, 2n)$ measurement method we had developed, and to primarily study the collection mechanism of recoil nuclei at several energies of incident neutrons. Section IV is dedicated to the determination of the collection efficiency in the $^{239}$Pu$(n, 2n)\,^{238}$Pu reaction by means of a measurement performed at the neutron energy around 9.3 MeV, taken as a reference point. This efficiency is then used to determine the cross-section data from measurements undertaken at neutron energies of 7.1 and 7.7 MeV as described in Sec. V. The results obtained in this paper are presented in Sec. VI, compared to previous experiments and to some available evaluations. This paper ends with a short conclusion set out in Sec. VII.

## II. RECOIL TECHNICS AND EXPERIMENTAL SYSTEMS

### A. A neutron production-gaseous target

The $(n, 2n)$ experiments on $^{239}$Pu were performed at the 7 MV Tandem Van de Graaff accelerator facility of the CEA-DAM Ile de France. Incident neutrons of 7.1, 7.7, and 9.3-MeV energy were produced via the $^{2}$H$(d, n)\,^{3}$He reaction with deuterons accelerated at energies between 4.5 and 6.7 MeV. At such energies, the neutron flux is primary directed to forward angles in the direction of the target samples with maximal energy at 0°. The beam intensity reached up to 20$\mu$A*e* on target during a few hundred hours. To obtain a sufficiently high neutron flux, we designed and developed a gaseous target which, associated with the high-current

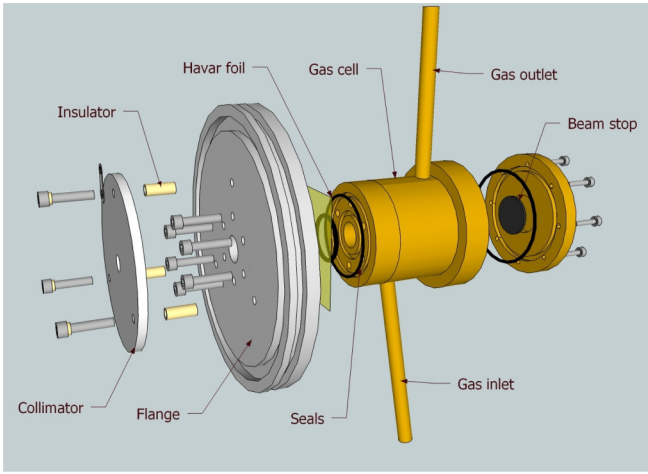


FIG. 2. Scheme of the gas target with the different elements.

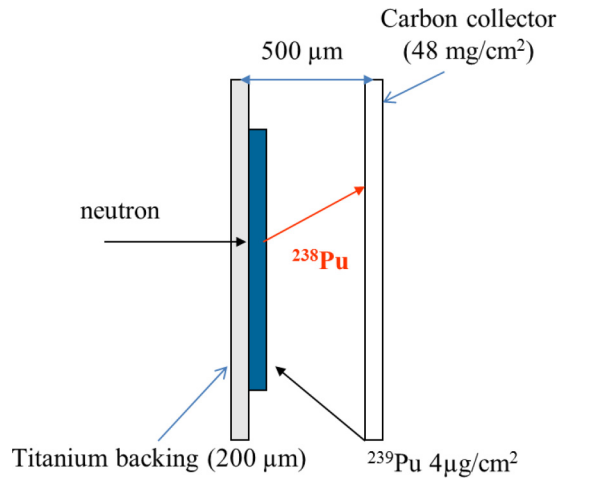


FIG. 3. The recoil device composed of the plutonium deposit and the carbon collector.

deuteron beam, could produce a flux of some $10^8$ n/cm$^2$/s on the target samples of $^{238}$U and $^{239}$Pu.

The ($n$, 2$n$) measurements on $^{238}$U were taken at four neutron energies: two at 7 and 8 MeV using the 7 MV Tandem Accelerator presented above, and the two others with neutrons of 15.3 and 15.8 MeV, produced via the $^3$H($d$, $n$) $^3$He reaction by using two electrostatic accelerators, one of 500-kV, the other of 4-MV voltages, respectively. Details on the choice of the energies and the accelerators will be given in Sec. III.

The incident neutrons supplied for the $^{238}$U and $^{239}$Pu experiments carried out with the Tandem accelerator were produced with the same gas target, which is presented hereafter.

The deuterium gaseous target was designed to satisfy several criteria: minimal neutron energy dispersion, high gas pressure to obtain high neutron flux, high mechanical strength of the accelerated deuteron beam entrance window to withstand high beam currents, and high target pressures.

Figure 2 shows an exploded view of the gaseous target. It was composed of a right cylinder of copper, which has an excellent thermal conductivity, a Havar® entrance window of 1-cm diameter, 5-$\mu$m thickness, and a 1-mm tantalum disk beam stop at the back of the cell. The target cell had an active length of 4.5 cm. The thickness of the gas cell on the plutonium sample side was 2 mm. It could support up to 3 bars of absolute pressure and a 20 $\mu$A$e$ beam current. An efficient device for cooling the target window has been developed: (i) The gas was cooled using a heat exchanger via a sealed gas circulator, (ii) the copper cell was cooled by a surrounding coil in which refrigerated Coolanol® circulates at $-20$°C temperature, (iii) an external air jet was directed toward the back of the target cell to aid its cooling. Temperature and pressure measurements were made in front and behind the gas target cell. Their values could be stored at a chosen periodicity in order to track any changes in the gas system during experiments. More details could be found in a future publication dedicated to the gaseous target and its in-beam tests [22].

In order to avoid hot spots on the entrance window, a beam profiler placed a few centimeters in front of a tantalum collimator upstream the gaseous target enabled to control the beam profile on the plane transverse to the beam axis.

### B. Recoil technique and counting assembly

The recoil technique was intensively used in various contexts in order to improve the signal-to-background ratio by collecting the recoil nucleus on a catcher foil. For instance, the discovery of mendelevium was performed using such a technique [23]. More recently, this technique was used in the study of superheavy elements [24]. However, few works use this method to extract cross sections of nuclear reactions [25–28]. To our knowledge, this method has not yet been applied to extract a neutron cross section.

In the present paper, the recoil device for $^{239}$Pu measurements consists of a thin deposit of $^{239}$PuO$_2$ electroplated on a titanium backing and associated with a carbon catcher situated in direct view of the deposit. A schematic of this recoil device is shown in Fig. 3.

This device is placed in an intense flux of neutrons for irradiation. The $^{238}$Pu recoiling nuclei produced by the ($n$, 2$n$) reaction are collected on the carbon catcher. After irradiation, the catcher is $\alpha$ counted to measure the $^{238}$Pu activity. However, all $^{238}$Pu recoiling nuclei do not reach the catcher, for reasons that are developed below. This implies that the collection efficiency of the recoil device must be determined. The only way to get this efficiency is to use previously published data. A standardization procedure is then mandatory. Although our measurements using the recoil method will not provide data with absolute values, they will, however, be compared to previous data and evaluations and allow to test for consistency.

The thickness of the $^{239}$PuO$_2$ deposit in the recoil device should be optimized to get a compromise between an optimal collection efficiency and an acceptable counting rate. At the lowest incident neutron energy in this paper, i.e., 7.1 MeV, the recoil kinetic energy of the $^{238}$Pu nuclei is the weakest, and its distribution is centered at 26 keV. Knowing that the mean range of the recoil $^{238}$Pu nuclei in PuO$_2$, calculated using the

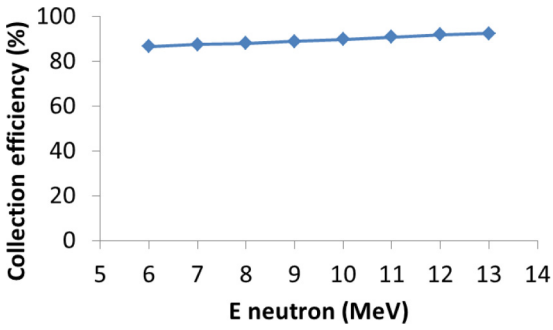


FIG. 4. Calculated collection efficiency of the $^{238}$Pu nuclei produced in the $^{239}$Pu$(n, 2n)$ as a function of the incident neutron energy for a 6-$\mu$g/cm$^2$PuO$_2$ matrix.

SRIM code [29], was estimated to be 6 $\mu$g/cm$^2$, we adopted a deposit thickness around 4 $\mu$g/cm$^2$ for our experiments.

We developed a Monte Carlo code to calculate the kinetic-energy distribution of the $^{238}$Pu recoiling nuclei supposed uniformly implanted in a 6-$\mu$g/cm$^2$PuO$_2$. The calculation considered the sizes of the neutron source and of the plutonium deposit, the angular distribution of the neutrons produced by the $^2$H$(d, n)^3$He reaction and the residual vacuum between the deposit and the collector. Distributions of the position and velocity vectors of the $^{238}$Pu nuclei were then used as inputs for the SRIM code. Figure 4 shows the collection efficiency calculated as a function of the incident neutron energy. This efficiency is slightly dependent on the incident neutron energy with a slope of 0.86%/MeV. However, calculation of this efficiency may be questionable for an electroplated deposit because of the strong influence of its surface roughness, tricky to estimate at the nanometer scale.

The constraint imposed on the thickness of the $^{239}$Pu deposit ($\sim$4$\mu$g/cm$^2$) as established above, implies that the production rate of recoil nuclei is not high enough to produce data with acceptable quality. Thus, in order to increase the production of recoil nuclei, we have designed a $^{239}$Pu target consisting of a stack of ten recoil devices. A schematic of the experimental setup is shown in Fig. 5.

TABLE I. Energy and relative intensity of the $\alpha$ transitions [30] for the isotopes involved in this paper. The isotopes are ordered by their $\alpha$-particle decay energies to indicate possible overlaps in the $\alpha$-particle spectra.

| | Energy (keV) | Intensity (%) |
|---|---|---|
| $^{239}$Pu | 5105. 8 | 11.94 |
| | 5144.3 | 17.11 |
| | 5156.59 | 70.77 |
| $^{240}$Pu | 5123.68 | 27.10 |
| | 5168.17 | 72.8 |
| $^{238}$Pu | 5456.33 | 28.98 |
| | 5499.03 | 70.91 |
| $^{241}$Am | 5442.8 | 13.1 |
| | 5485.56 | 72.80 |

### C. Plutonium and uranium deposits

A 1 ml of Pu$(NO_3)_4$ solution, enriched at 97.94% in $^{239}$Pu atoms with 2% of $^{240}$Pu nuclei and the remainder consisting of other plutonium isotopes, $^{238,241}$Pu, and $^{241}$Am nuclei, was developed to be electrodeposited on the ten titanium backings of the target stack. But, because the $\alpha$-decay lines of $^{241}$Am contained in the solution cannot be separated from those of $^{238}$Pu (Table I), this solution was partially depleted in $^{241}$Am by a chemical process before electrodeposition. Additionally, nitrate ions present in this solution were discarded by adding to it 0.5 ml of concentrated hydrochloric acid. Finally, 10 ml of a 5.5-M $NH_4Cl$ solution at *p*H 1 was added to the plutonium solution to elaborate the plating electrolyte solution. This purified solution was then electrodeposited on the backings inside an electrochemical cell at a constant density of charge (e.g., $I = 1.5$ A, $V < 20$ V) for 30 min. The titanium backings were disks of 25-mm diameter and 200-$\mu$m thickness, and the diameter of the centered plutonium deposits was 15 mm. After electroplating, each backing was evaporated to dryness, then carefully washed, first with alcohol and then with water, and finally heated to fix $PuO_2$ onto the backing.

Each deposit has been characterized by $\gamma$ spectroscopy (Fig. 6) to obtain the $^{240}$Pu/$^{239}$Pu and $^{241}$Am/$^{239}$Pu

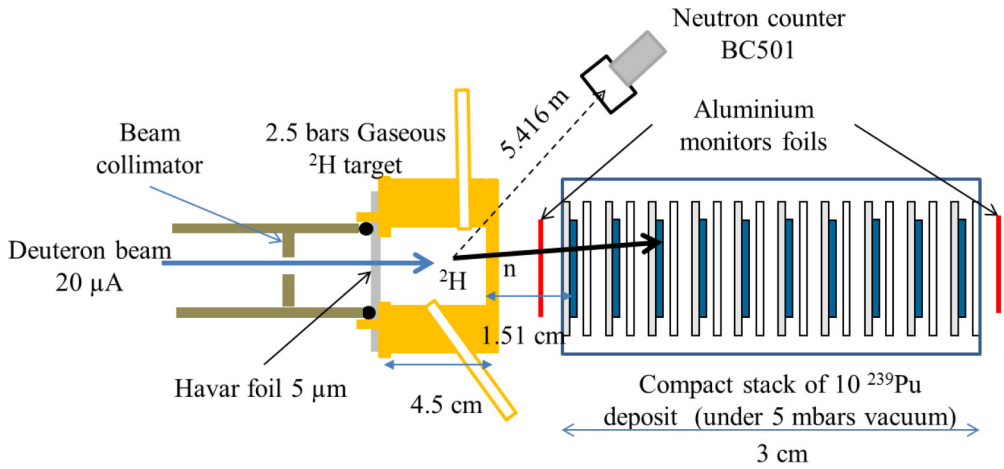


FIG. 5. Schematic (not to scale) of the experimental setup.

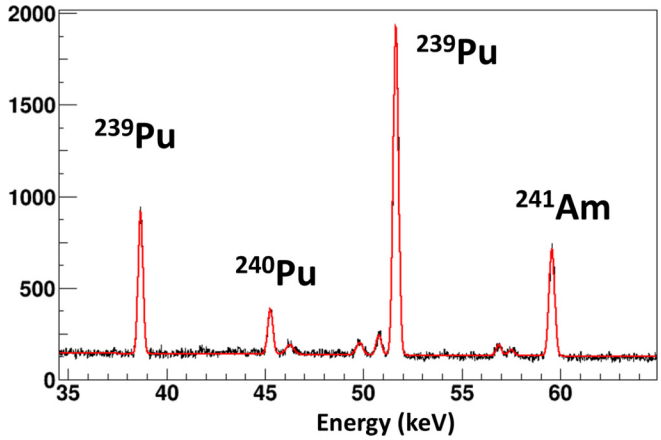


FIG. 6. $\gamma$ spectroscopy of a plutonium sample before irradiation. The red line is a fit of the spectrum.

atom-number ratios. Amounts of $^{239}$Pu and $^{238}$Pu nuclei have been measured by $\alpha$ spectroscopy. The remaining amounts of $^{240}$Pu and $^{241}$Am contaminating the $\alpha$ peaks of $^{239}$Pu and $^{238}$Pu, respectively (Table I) were subtracted using the measured ratios. Table II gives the amount of the isotopes relative to the $^{239}$Pu.

Table III gives the $^{239}$Pu mass for each deposit. The weighted average ratios of atom numbers for $^{238}$Pu/$^{239}$Pu and $^{241}$Am/$^{239}$Pu were estimated at $(1.96 \pm 0.03) \times 10^{-5}$ and $(4.95 \pm 0.03) \times 10^{-6}$, respectively.

For the study of the $^{238}$U($n$, 2$n$) $^{237}$U reaction (see Sec. III) two recoil devices, the same as those used for the $^{239}$Pu study but containing thin $^{238}UO_2$ deposits ($3.84 \pm 0.12$ $\mu$g and $3.33 \pm 0.54$ $\mu g$ ) were made using the same titanium backings and carbon collectors. The $^{238}UO_2$ target fabrication procedure was similar to that used for $PuO_2$ but simpler because the $UO_2$ solution was very pure. The depth of uranium inside titanium was measured by Rutherford backscattering (RBS). This depth was estimated using the code SIMNRA® [31] to have an average value of 20 Å with a standard deviation of 20 Å. The mass of the uranium deposits was measured by means of $\alpha$-ray spectrometry. Mass values of the two deposits are given in Table IV.

### D. Target holder-reaction chamber

The recoil devices, ten for plutonium, one or two for uranium, were placed in a very compact assembly which had to be positioned as close as possible to the neutron-production target for maximal irradiation. Each recoil device consisted of a 320-$\mu$m-thick vitreous carbon foil ($2.5 \times 3$ cm) which was placed at a distance of 500 $\mu$m behind the active deposit, relative to the direction of the incident neutrons, to collect the recoiling nuclei ($^{238}$Pu or $^{237}$U). Each recoil device, with its deposit-collector couple, was housed in a specially designed small-size support. The supports were stacked in a basket, which was then positioned in an aluminum reaction chamber (Fig. 7). The chamber length (3 cm) was as small as possible in order to minimize the distance between the gaseous target and the deposits along the beam direction and, thus, to increase the neutron flux on the stack. The supports were separated by about 2 mm and, for the plutonium stack, the first and last deposits were positioned at 1.51 and 3.76 cm, respectively, from the bottom of the gas cell.

Two aluminum disks ($\varnothing = 15$ mm) placed in front and behind the reaction chamber with respect to the beam axis are used to monitor the neutron flux. During irradiation, the chamber was connected to a vacuum pump which maintained the vacuum at a pressure of 5 mbars of air in order to minimize the sputtering of the target under neutron bombardment. Indeed, the sputtering process can eject $^{238}$Pu atoms from the target onto the collector which is then contaminated. The choice of this pressure value fulfills the compromise between an efficient attenuation of the sputtered nuclei, determined by a measurement using a $^{239}$Pu source and a good transmission of the nuclei produced by the ($n$, 2$n$) reaction on $^{239}$Pu.

During measurements the chamber, supported by a three-dimensional-printed frame, was positioned behind the gaseous

TABLE II. Amount of isotopes present in deposits relative to $^{239}$Pu.

| Isotope | Relative amount (%) | Relative to $^{239}$Pu |
|---|---|---|
| Pu-238 | $1.92 \times 10^{-3}$ | $(1.96 \pm 0.03) \times 10^{-5}$ |
| Pu-239 | 97.941 | 1 |
| Pu-240 | 2.10 | $(2.15 \pm 0.02) \times 10^{-2}$ |
| Am-241 | $4.85 \times 10^{-3}$ | $(4.95 \pm 0.03) \times 10^{-6}$ |

TABLE III. $^{239}$Pu mass of samples.

| Sample position inside the chamber | Mass $^{239}$Pu ($\mu$g) |
|---|---|
| 1 | $8.40 \pm 0.04$ |
| 2 | $6.97 \pm 0.05$ |
| 3 | $6.72 \pm 0.05$ |
| 4 | $5.85 \pm 0.03$ |
| 5 | $5.55 \pm 0.03$ |
| 6 | $5.29 \pm 0.04$ |
| 7 | $5.84 \pm 0.05$ |
| 8 | $6.51 \pm 0.04$ |
| 9 | $6.80 \pm 0.04$ |
| 10 | $7.44 \pm 0.05$ |

TABLE IV. Collection efficiencies in $^{238}$U($n$, 2$n$) $^{237}$U for two electrodeposits and in $^{197}$Au($n$, 2$n$) $^{196}$Au for the evaporated gold deposit.

| Isotope | Mass ($\mu$g) | Neutron energy (MeV) | Collection efficiency (%) |
|---|---|---|---|
| $^{238}$U | $3.84 \pm 0.12$ | 7 | $38 \pm 4$ |
| | $3.33 \pm 0.54$ | | $49.5 \pm 8.5$ |
| | $3.84 \pm 0.12$ | 8 | $44.6 \pm 4.5$ |
| | $3.33 \pm 0.54$ | | $41 \pm 7$ |
| | $3.84 \pm 0.12$ | 15.3 | $48 \pm 5$ |
| | $3.33 \pm 0.54$ | 15.8 | $62 \pm 18$ |
| $^{197}$Au | $9.0 \pm 0.4$ | 15.8 | $115 \pm 20$ |

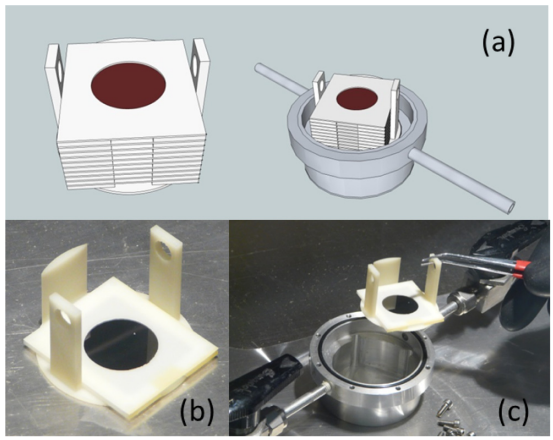


FIG. 7. (a) Drawing of the stack of ten deposit-collector couples inside the basket. (b) Photograph of the basket with a deposit-collector device. (c) Photograph of the basket positioning inside the irradiation chamber.

target as shown in Fig. 8. The two aluminum disks which monitored the neutron flux were fixed on a removable holder shown in red in Fig. 8. This setup enables to accurately position the aluminum disks at 0.4 and 4.7 cm from the gas cell end, and it allows to easily remove the disks every day for $\gamma$ counting without dismantling the entire configuration.

### E. Neutron flux monitoring

In experiments where neutrons were produced by the $^{2}$H$(d, n)$ $^{3}$He reaction, the neutron flux was monitored by two

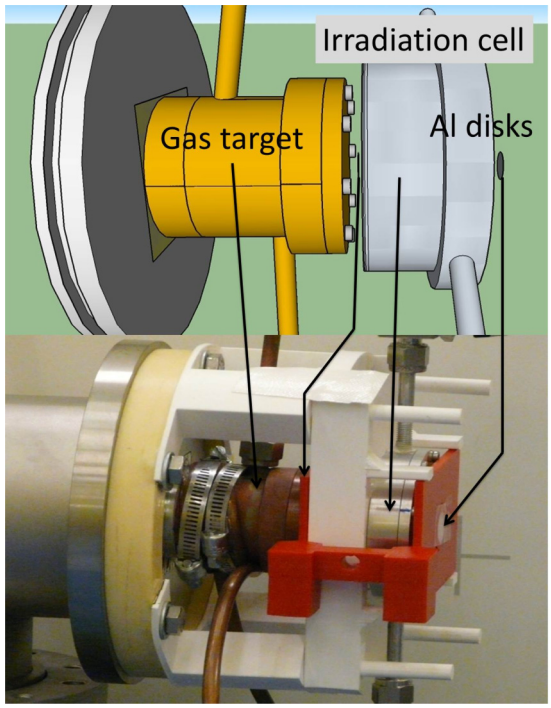


FIG. 8. Drawing (on the top) and a photograph (on the bottom) of the irradiation cell sited on the gaseous target.

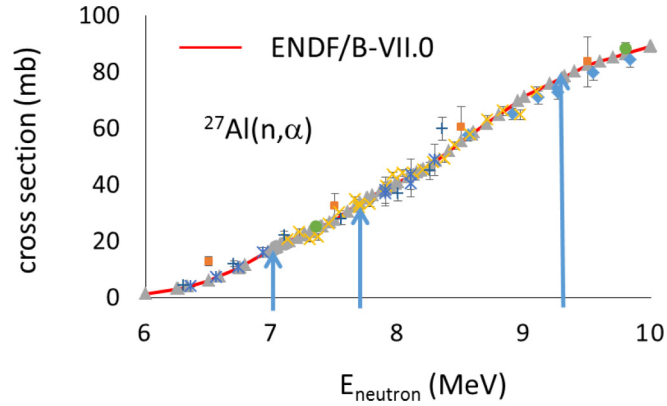


FIG. 9. $^{27}$Al$(n,\alpha)$ cross section. Experimental data are from EXFOR. The red curve is the ENDF/B-VII.0 evaluation used in the analysis. The blue arrows correspond to the incident neutron energies in this paper.

aluminum foils each of (98.5 $\pm$ 0.1)-mg mass using the standard reaction $^{27}$Al$(n,\alpha)$ $^{24}$Na. Figure 9 shows the $^{27}$Al$(n,\alpha)$ $^{24}$Na cross section of the END/F BVIII.0 evaluation used in the analysis, compared to the more recent data from the EXFOR database [32]. Comparison of the evaluation with the nuclear data shows an uncertainty of 1%, which value was considered in the final analysis.

Every day, after an irradiation lasting a few hours, the beam was turned off and the aluminum foils were $\gamma$ counted using two high-purity germanium detectors (HPGe). The aluminum foils were placed in a plastic holder that ensured a very precise positioning with respect to the germanium detectors. The $^{24}$Na($t_{1/2}$ = 14.96-h) activities produced by the $^{27}$Al$(n,\alpha)$ $^{24}$Na reaction were extracted from the $\gamma$ spectra (Fig. 10). Before each irradiation period, a couple of new aluminum foils was put in place without moving the plutonium deposits. The accuracy on the aluminum foil repositioning, checked by a theodolite measurement, was better than 500 $\mu$m.

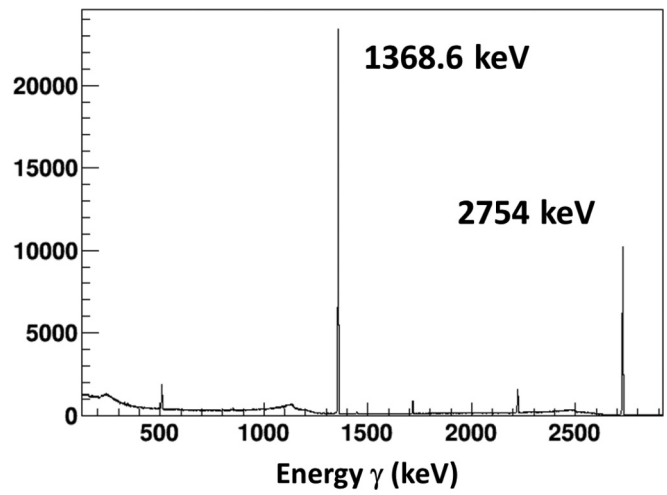


FIG. 10. $\gamma$-ray spectrum measured after irradiation of a sample aluminum monitor. The 1368.6- and 2754-keV $\gamma$-ray transitions come from the $\beta$ decay of $^{24}$Na.

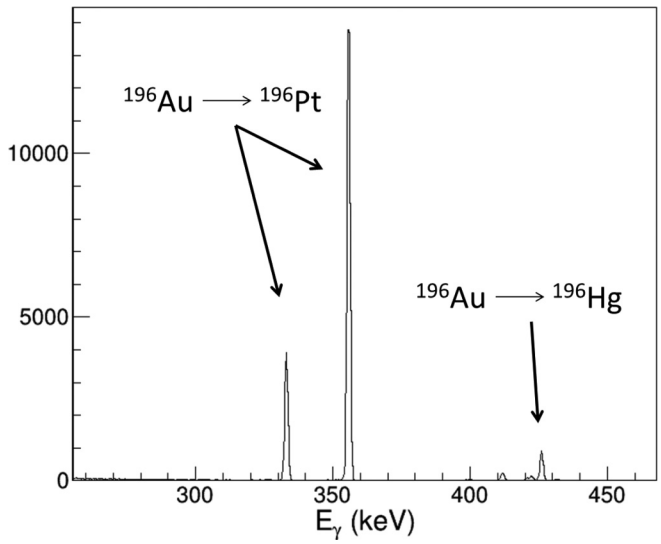


FIG. 11. $\gamma$-ray spectrum measured after irradiation of a gold monitor. The 426-keV $\gamma$-ray transition comes from the $\beta$ decay of $^{196}$Hg and the 333 and 356 keV from the *e.c.* decay of $^{196}$Pt.

The neutron flux produced by the $^{3}$H($d$, $n$) $^{3}$He reaction at 15.3 and 15.8 MeV, was monitored by two gold foils, using the standard reaction $^{197}$Au($n$, 2$n$) $^{196}$Au. After a few-days irradiation run, the $^{196}$Au($t_{1/2}$ = 6.16-d) activity of the foils were $\gamma$ counted using a HPGe detector. A measured $\gamma$-ray spectrum is shown Fig. 11.

Moreover, a BC501 liquid scintillator neutron detector (Fig. 5), located 5.416 m from the neutron source and 20° from the deuteron beam axis, enabled estimating corrections for time fluctuations of the neutron flux arising from variations in the beam intensity and the deuterium gas pressure. Figure 12 shows a typical variation of the number of neutrons detected by the BC501 during an irradiation day.

### F. $\alpha$ counting

After a few hundred hours of irradiation of the plutonium stack, the carbon collector of each recoil device was retrieved and put inside a spectrometer for $\alpha$ counting. Measurement of the $\alpha$ activity was performed using an $\alpha$Analyst spectrometer from Mirion®. It consisted of six independent

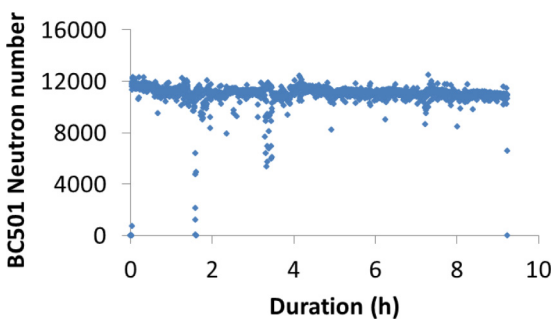


FIG. 12. Variation of the number of neutrons detected by the BC501 during an irradiation day. Each point corresponds to a 10-s period.

chambers, each of them with two measuring channels. The collectors were positioned 2.2 mm from the active surface of an A450 PIPS detector (passivated implanted planar silicon) with a surface area of 450 mm$^2$. This type of detector was optimized for high resolution (15-keV) and low background (<0.05-count/h/cm$^2$) spectroscopy in the 3–8-MeV energy range. The spectrometers were sited in an air-conditioned room to allow air renewal and low radon level which could contaminate the samples. The radon concentration was monitored, and its value recorded every 15 min. A channel of the $\alpha$ Analyst was dedicated to measurement and control of background noise. During all measurements, we did not observe any radon contamination.

The positioning of the collectors in the $\alpha$Analyst channels as well as the use of nonidentical PIPS could lead to differences in the efficiency. To estimate the differences, each carbon collector was measured several times on various $\alpha$Analyst channels, and the differences on the measured activities were found to be less than 1%.

## III. MEASUREMENTS OF THE COLLECTION EFFICIENCY USING THE $^{238}$U($n$, 2$n$) $^{237}$U REACTION

In order to understand as best as possible the collection mechanism in a recoil device, an experiment was undertaken which consisted of irradiating, at several energies, a set of three target samples: the two thin $^{238}$U deposit samples described above and a thick massive $^{238}$U sample. The collection efficiency for the $^{238}$U($n$, 2$n$) $^{237}$U reaction was then obtained by analyzing the ratio of collected activity from the thin deposit over the thick sample activity, normalized with respect to measured masses and neutron fluence by means of the code MCNP [33].

The short half-life of $^{237}$U($t_{1/2}$ = 6.75d) and the absence of native $^{237}$U nuclei in the samples make the $^{238}$U($n$, 2$n$) reaction a good candidate for studying the collection efficiency.

The thick $^{238}$U sample, a disk of 8-mm diameter, and (0.465 ± 0.009)-g mass, and the thin $^{238}$U deposits were positioned in the reaction chamber, described above (Sec. II D), evacuated also at a pressure of 5 mbars for the irradiation runs. The mass of the thick $^{238}$U sample was obtained by $\gamma$-ray spectroscopy where the photon absorption inside the sample was considered through a GEANT4 simulation. This value agreed with that obtained by a measurement of the mass by weighing.

The thin and thick samples were irradiated at the neutron energies of 7, 8, 15.3, and 15.8 MeV. The first two energies were chosen to be close to those used in the irradiation of plutonium deposits (7.1, 7.7, and 9.3 MeV). Both highest energies of 15.3 and 15.8 MeV were chosen to study the variation of the collection efficiency over a wide energy range.

The 7 MV Tandem accelerator, located at CEA DAM Ile de France, was used to produce neutrons of 7- and 8-MeV energy via the $^{2}$H($d$, $n$) $^{3}$He reaction.

The neutrons of 15.3-MeV energy were produced via the $^{3}$H($d$, $n$) $^{4}$He reaction on a thick tritium-adsorbed tantalum disk and using the 500-kV Van de Graaff accelerator located at the Valduc CEA research center (Dijon, France).

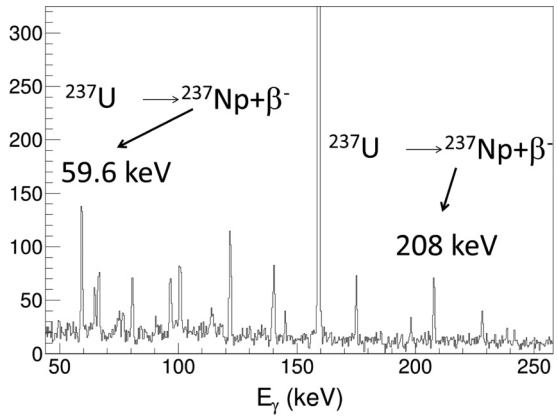


FIG. 13. $\gamma$-ray spectrum of a carbon collector following the irradiation of a thin $^{238}$U deposit induced by 15.3-MeV neutrons. The 59.6- and 208-keV $\gamma$-ray transitions come from the $\beta$ decay of $^{237}$U with the relative intensity of $(34.5 \pm 0.8)\%$ and $(21.2 \pm 0.3)\%$ [30], respectively. The other peaks come from the radioactive scandium nuclei collected after being produced by the interaction of neutrons and the titanium backing.

The 15.8-MeV neutrons were produced, via the $^3$H$(d, n)$ $^4$He reaction on also a thick tritium-adsorbed tantalum disk and using the 4 MV Van de Graaff accelerator located at CEA DAM Ile de France at the deuteron energy of 500 keV. The same setup and measurement protocol were used in all experiments.

For the 15.3- and 15.8-MeV measurements, two thick gold foils were placed in front and behind the reaction chamber in order to monitor the neutron flux. For measurements at 7 and 8 MeV the gold foils were replaced by two thick aluminum foils, the same as in the $^{239}$Pu experiment, which are better suited for monitoring neutrons at these energies.

The low activity of the carbon-foil collectors, containing the recoil $^{237}$U nuclei outgoing from the thin targets was measured using an ultralow-background $\gamma$-ray spectrometer [34] (Fig. 13). Activities of the thick $^{238}$U sample and the monitor foils were carefully measured with a standard HPGe detector.

Measurement results are summarized in Table IV. The measured collection efficiency depends only slightly on the neutron energy as observed in Fig. 14. However, these measured data are twice as low as the estimated values (Fig. 4).

To check the origin of this discrepancy, a new irradiation measurement was performed at 15.8-MeV neutron energy using the 4 MV accelerator via the $^3$H$(d, n)$ $^4$He reaction at 500-keV deuteron energy. The recoil device with the $(3.33 \pm 0.54)$-$\mu$g uranium deposit, and a thin deposit of $^{197}$Au was positioned behind the neutron target. Comparison of the collection efficiencies extracted from the $(n, 2n)$ reaction on $^{238}$U and $^{197}$Au would help clarify the mechanism of collection. The $^{197}$Au deposit consisted in a metal evaporation of $23 \pm 1$-Å thickness on the backing, as indicated by an RBS measurement. These thin $^{238}$U and $^{197}$Au deposits together with the same thick $^{238}$U sample as used in previous experiments were placed in the reaction chamber for irradiation. Neutron flux monitoring was achieved by using two gold foils. These foils served also with the thin gold deposit to extract the collection efficiency in the $^{197}$Au$(n, 2n)$ $^{196}$Au$(t_{1/2} = 6.16$-d$)$ reaction.

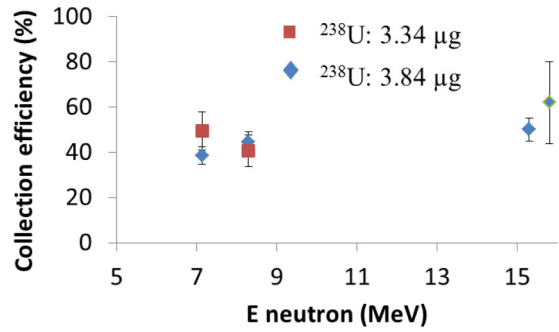


FIG. 14. Collection efficiency for the $^{238}$U$(n, 2n)$ $^{237}$U vs neutron energy for two uranium deposits. The red squares correspond to the $(3.33 \pm 54)$-$\mu g$ sample, and the blue diamonds correspond to the $(3.84 \pm 12)$-$\mu g$ sample.

The measured efficiencies obtained in this new experiment were $(62 \pm 18)\%$ and $(115 \pm 20)\%$ for the $^{238}$U$(n, 2n)$ $^{237}$U and $^{197}$Au$(n, 2n)$ $^{196}$Au reactions, respectively. Figure 14 shows the variation of the collection efficiency for the $^{238}$U$(n, 2n)$ $^{237}$U reaction as a function of the neutron energy. The result at 15.8 MeV for the $^{238}$U deposit is in good agreement with the previously measurement performed at 15.3 MeV. For the gold deposit the value obtained at 15.8 MeV is very close to the collection efficiency calculated with SRIM [29] for a homogeneously evaporated mass on the backing surface. These results point out that the inhomogeneity of the $^{238}$U electrodeposits is responsible for the low values of the collection efficiency. Therefore, we cannot rely on the calculation and a measurement is mandatory.

## IV. COLLECTION EFFICIENCY IN THE $^{239}$Pu$(n, 2n)$ $^{238}$Pu REACTION

The measurement of the collection efficiency in the $^{238}$U$(n, 2n)$ $^{237}$U reaction showed that the strong inhomogeneity of the deposits prevented a precise calculation of this efficiency. In order to extract the collection efficiency in $^{239}$Pu$(n, 2n)$ $^{238}$Pu, a measurement was performed at the energy of $E_n \approx 9.3$ MeV$(E_{\text{deuteron}} = 6.68$ MeV$)$ at which all available data and evaluations of the $(n, 2n)$ cross section are in good agreement (Fig. 1). The data published prior to this paper, thus, allowed us to extract the value of the collection efficiency of each of the deposits, which then was used for the analysis of lower-energy data.

The plutonium deposits were irradiated during 100 h by a neutron flux which was monitored with two aluminum foils as described above in Sec. II.

Figure 15(a) shows the $\alpha$ spectrum emitted by a plutonium sample before irradiation. Figure 15(b) shows the $\alpha$ spectrum of the collector located behind this plutonium sample, measured after an irradiation at 9.3 MeV lasting 127 h. The $\alpha$ activity on the collector was measured over a 112-d duration period. The resolution is better for the deposit measurement

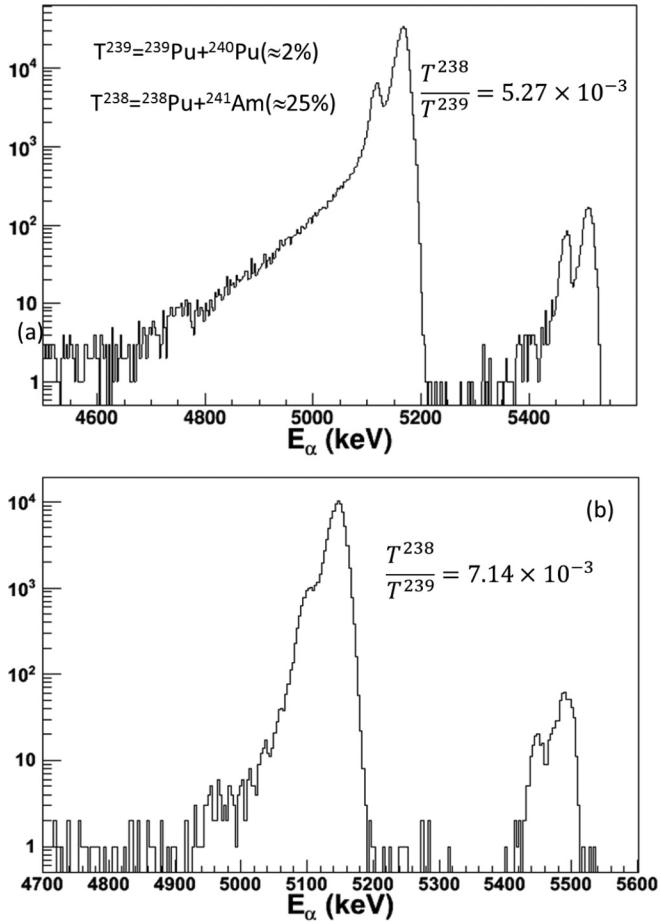


FIG. 15. (a) $\alpha$ spectrum before irradiation for a plutonium sample. (b) $\alpha$ spectrum for its associated collector after 127-h irradiation at 9.3-MeV neutron energy and 112-days activity measurement. The $T^{238}/T^{239}$ ratio is given for the two spectra.

[Fig. 15(a)] because the distance between the deposit and the silicon detector is 8 cm compared to 2.2 mm for the collector. Both spectra exhibit two $\alpha$ groups. The first one, around the energy of 5.1 MeV and named $T^{239} = {}^{239}$Pu+$^{240}$Pu in Fig. 15(a), represents the $\alpha$ emission of $^{239}$Pu (98%) and $^{240}$Pu (2%), see above Sec. II; on the collector, it yields an $\alpha$ activity of $(12.20 \pm 0.03)$ mBq. The second group, around the energy of 5.5 MeV and named $T^{238} = {}^{238}$Pu + $^{241}$Am, represents the $\alpha$ emission of $^{238}$Pu (75%) and $^{241}$Am (25%). On the collector, it yields an $\alpha$ activity of $(0.0875 \pm 30)$ mBq. For the collector, the $T^{239}$ activity originated from the plutonium atoms sputtered from the target to the collector. The expected activity due to the neutron elastic and inelastic scatterings on $^{239}$Pu is about $10^{-3}$ mBq and could, thus, be neglected. As $^{238}$Pu and $^{241}$Am nuclei were also present in the plutonium deposits, the amount of these sputtered nuclei had to be subtracted from the total amount $T^{238}$ to obtain the amount of $^{238}$Pu nuclei coming only from the ($n$, 2$n$) reaction. The quantity to be subtracted was obtained from the knowledge of both the $T^{239}$ activity and the ratio of $T^{238}/T^{239}$ weighted activities of the ten plutonium deposits, and it has been measured to be $(5.27 \pm 0.03) \times 10^{-3}$. The activity of $^{238}$Pu nuclei produced by the ($n$, 2$n$) reaction is then,

$$A_{\text{total}}^{^{238}\text{Pu}} = \text{T}^{238} - \text{T}^{239} \times 5.27 \times 10^{-3}. \tag{1}$$

The total $^{238}$Pu activity produced by the ($n$, 2$n$) reaction, at the end of an irradiation run is given by

$$A_{\text{total}}^{^{238}\text{Pu}} = \frac{\ln 2}{t_{1/2}^{^{238}\text{Pu}}} \varepsilon_{\text{coll}} \frac{N_A M}{A} \iint dt\, dE\, \phi[E, P(t), I(t)]\sigma(E), \tag{2}$$

where $t_{1/2}^{^{238}\text{Pu}}$ is the $^{238}$Pu half-life, $\varepsilon_{\text{coll}}$ is the collection efficiency, $N_A$ is the Avogadro number, $M$ is the mass of the $^{239}$Pu deposit, $A$ is the atomic mass number, $\sigma(E)$ is the ($n$, 2$n$) cross section at the incident-neutron energy $E$, and $\phi[E, P(t), I(t)]$ is the neutron-flux per energy bin $dE$, which depends on the energy $E$, on the time-dependent parameters $P(t)$, pressure of the gaseous target, and $I(t)$ the current intensity of the accelerated deuterons. During the irradiation runs the pressure was retained within $2.5 \pm 0.1$ bars, affording to neglect its variations estimated to be 2%/bars on the final result. We write then $\phi[E, P, I(t)] \equiv \phi_P[E, I(t)]$.

Considering that the total duration of the run is divided in short intervals of equal duration $\Delta t_{\text{irr}}$ (typically 10 s) and that for the entire duration of each interval $i$ the neutron flux is constant, the total $^{238}$Pu activity, which is the sum of partial activities of all the intervals $i$ in the run, can then be written as

$$A_{\text{total}}^{^{238}\text{Pu}} = \frac{\ln 2}{t_{1/2}^{^{238}\text{Pu}}} \varepsilon_{\text{coll}} \lambda_{n,2n} \Delta t_{\text{irr}} \sum_i N_n(I_i). \tag{3}$$

Since the reaction rate $\lambda_{n,2n}$ is given per source neutron, it does not depend on the deuteron beam current and, thus, could be factorized out of the sum in Eq. (3).

$N_n(I_i)$ is the number of emitted neutrons during the bin $i$, determined from the activity of the aluminum foils measured every day after a few 10 h of irradiation; it is determined through the following relation:

$$A^{^{24}\text{Na}} = \lambda_{n\alpha} \frac{\ln 2}{t_{1/2}^{^{24}\text{Na}}} \Delta t_{\text{irr}} \sum_i e^{-\lambda_{^{24}\text{Na}} \Delta t_c^i} N_n(I_i), \tag{4}$$

where $\Delta t_c^i$ is the time separating the bin $i$ from the end of the run, $\lambda_{n\alpha}$ is the $^{27}$Al($n$,$\alpha$) $^{24}$Na reaction rate per source neutron, and $t_{1/2}^{^{24}\text{Na}}$ is the $^{24}$Na half-life.

The collection efficiency can be extracted from the $^{238}$Pu and $^{24}$Na activities by using the relation,

$$\varepsilon_{\text{coll}} = \frac{t_{1/2}^{^{238}\text{Pu}}}{t_{1/2}^{^{24}\text{Na}}} \frac{\lambda_{n,\alpha}}{\lambda_{n,2n}} \frac{1}{\sum_j \frac{A_j^{^{24}\text{Na}}}{A_{\text{total}}^{^{238}\text{Pu}}} f_{\text{BC501}}^j}, \tag{5}$$

where the index $j$ in Eq. (5) represents the successive measurements of the aluminum foils performed each day, $f_{\text{BC501}}^j = [\frac{\sum_i N_i^{\text{BC501}}}{\sum_i (e^{-(\ln 2/t_{1/2}^{^{24}\text{Na}})\Delta t_c^i} N_i^{\text{BC501}})}]_j$ is a factor that accounts for beam current variation, and $N_i^{\text{BC501}}$ is the neutron number measured with the BC501 counter during the bin $i$ (see Sec. II). The statistical uncertainty on $f_{\text{BC501}}^j$ is less than 0.01% and will be neglected in the following.

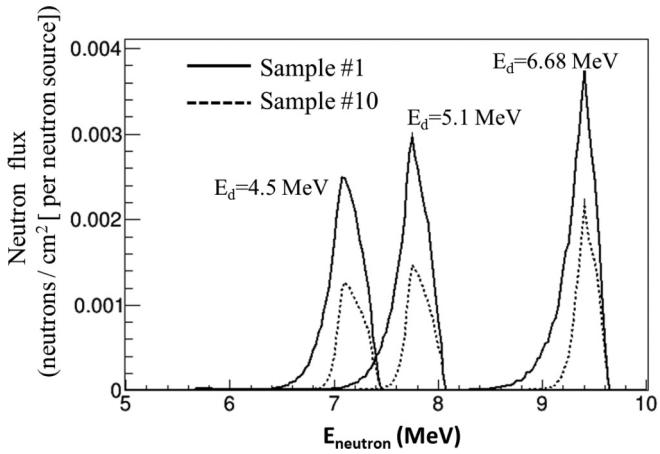


FIG. 16. Calculated neutron fluences on the first and last samples for the three deuteron energies of the experiment at the gas pressure of $P = 2.5$ bars.

The reaction rates $\lambda_{n,\alpha}$ and $\lambda_{n,2n}$ at $E \approx 9.3\,\mathrm{MeV}(E_{\mathrm{deuteron}} = 6.68\,\mathrm{MeV})$ are obtained from a simulation using the previously published cross sections. The compactness of the experimental setup and its close proximity to the neutron source require a complete simulation that was performed with MCNP [33] coupled with the NEUSDESC code [35] for the source definition. NEUSDESC uses the $^2\mathrm{H}(d,n)^3\mathrm{He}$ cross section database at various deuteron energies, pressures, and lengths of the gas cell. The two-dimensional distribution of the deuteron beam as measured with a beam profiler positioned just upstream from the gas cell has been added to the other input parameters in the simulation codes. Figure 16 shows the neutron fluences per source neutron at gas pressure $P = 2.5$ bars, calculated for the first and last deposits at the three deuteron energies of this paper. The neutron energy spread on the target samples originates from the kinematics of the $^2\mathrm{H}(d,n)^3\mathrm{He}$ reaction, the extended geometries of the gas cell and the plutonium deposits, and the distances separating them. The smaller this distance and the lower the deuteron energy, the greater the spread.

In order to check for the reliability of the experimental method we developed and to increase the counting statistics, two irradiation runs were performed at the deuteron energy $E_d = 6.68\,\mathrm{MeV}$, corresponding to the average neutron energy of 9.3 MeV on the plutonium samples with respective durations of 191.5 and 127.5 h. These measurements were taken at 3-month intervals. After irradiation, measurements of the $\alpha$ activities lasted 292.5 and 330 days, respectively. Figure 17(a) shows, for both irradiations, the measured collection efficiencies (blue and red dots, respectively) for each plutonium deposit numbered from 1 to 10 (see Table II). Error bars in this plot reflect only the statistical uncertainties. The two measurements are in very good agreement with each other. The weighted average efficiency of the two data sets is plotted in Fig. 17(b). This figure clearly shows important fluctuations between the ten deposits which require determining the efficiency for each of them. Collection efficiencies for the $^{239}$Pu deposits are quite similar to those for the $^{238}$U deposits presented above. The latter shows that

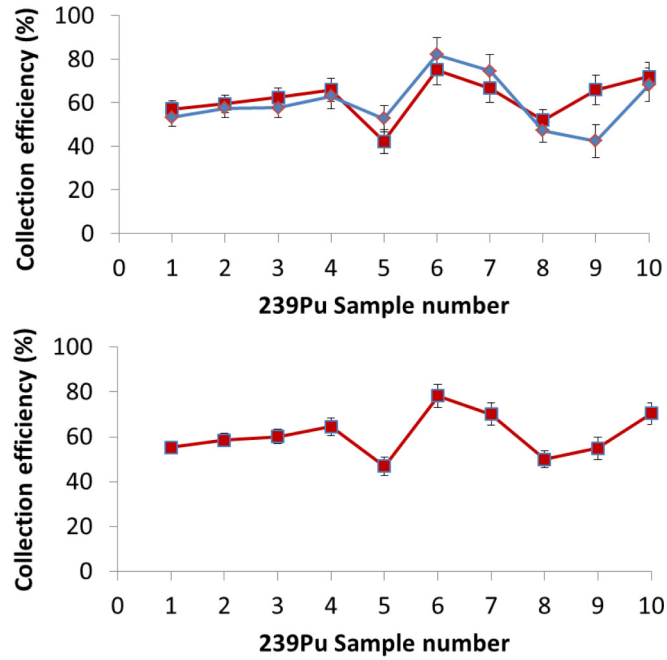


FIG. 17. (a) Comparison of collection efficiencies obtained for two periods of irradiation. (b) Weighted average efficiency. The neutron energy is 9.3 MeV.

the collection efficiency varies slightly from 7 MeV up to 15 MeV, and we assume this holds for the plutonium deposits between 7.1 and 9.3 MeV. The code TRIM indicates a relative difference of about 1.8% between the efficiencies at 7.1 and 9.3 MeV. The uncertainty arising from this assumption supported by the TRIM calculation is most likely less than the uncertainties of the measurements. Using the data and their associated uncertainties given in Table IV, we adopted a relative systematic error of 4% for the $^{238}$Pu collection efficiency at 7.1 and 7.7 MeV.

### V. $^{239}$Pu$(n, 2n)$ CROSS SECTIONS AT 7.1 AND 7.7 MEV

Using the collection efficiency obtained at $E_d = 6.7\,\mathrm{MeV}(E_n \approx 9.3\,\mathrm{MeV})$, two irradiations were performed, one at $E_d = 4.5\,\mathrm{MeV}(E_n \approx 7.10\,\mathrm{MeV})$ and the other at $E_d = 5.1\,\mathrm{MeV}(E_n \approx 7.72\,\mathrm{MeV})$ in order to determine the $^{239}\mathrm{Pu}(n,2n)$ cross sections in the region above the threshold of the reaction. The total activity on a collector after an irradiation with a deuteron beam of energy $E_d$ is then,

$$A^{^{238}\mathrm{Pu}}_{\mathrm{total}}(E_d) = \varepsilon_{\mathrm{coll}} \frac{\lambda_{^{238}\mathrm{Pu}}}{\lambda_{^{24}\mathrm{Na}}} \frac{t^{^{24}\mathrm{Na}}_{1/2}}{t^{^{238}\mathrm{Pu}}_{1/2}} \frac{\lambda_{n2n}(E_d)}{\lambda_{(n,\alpha)}(E_d)} \times \sum_j A^{^{24}\mathrm{Na}}_j(E_d) f^j_{\mathrm{BC501}}(E_d). \quad (6)$$

Using Eq. (5), the $^{239}\mathrm{Pu}(n,2n)$ reaction rate per source neutron $\lambda_{n2n}(E_d)$ is written as

$$\lambda_{n2n}(E_d) = \lambda_{n2n}(E_d = 6.7\,\mathrm{MeV}) \times \frac{\lambda_{(n,\alpha)}(E_d)}{\lambda_{(n,\alpha)}(E_d = 6.7\,\mathrm{MeV})} R_A(E_d), \quad (7)$$

TABLE V. Parameters of both irradiations.

| | | Duration | |
|---|---|---|---|
| Deuteron energy(MeV) | Average neutron energy (MeV) | Effective irradiation (h) | Activation measurement (days) |
| 4.47 | 7.1 | 332.30 | 303 |
| 5.08 | 7.7 | 176 | 186 |

where

$$R_A(E_d) = \frac{A^{238\mathrm{Pu}}_{\mathrm{total}}(E_d)}{A^{238\mathrm{Pu}}_{\mathrm{total}}(E_d = 6.7\,\mathrm{MeV})} \times \frac{\sum_j A_j^{24\mathrm{Na}}(E_d{=}6.7\ \mathrm{MeV}) f^j_{\mathrm{BC501}}(E_d = 6.7\ \mathrm{MeV})}{\sum_j A_j^{24\mathrm{Na}}(E_d) f^j_{\mathrm{BC501}}(E_d)}. \quad (8)$$

The uncertainty on this quantity is strongly dominated by the statistical uncertainty arising from the $^{238}$Pu activity measurement. The use of standardization data points removes much of the systematic uncertainty (mass of deposit, $\gamma$ and $\alpha$ efficiencies, etc., …).

The average ($n$, 2$n$) cross section for each deposit was determined by means of the following relation:

$$\overline{\sigma}_{^{238}\mathrm{Pu}}(E_n) = \overline{\sigma}_{^{238}\mathrm{Pu}}(9.3\ \mathrm{MeV}) \frac{\overline{\phi}_{6.7\,\mathrm{MeV}}}{\overline{\phi}_{E_d}} \frac{\lambda_{(n,\alpha)}(E_d)}{\lambda_{(n,\alpha)}(6.7\,\mathrm{MeV})} R_A(E_d), \quad (9)$$

where $E_n = \frac{\int_{E_{\mathrm{thres}}}^{E_{\mathrm{max}}} \phi(E) E\, dE}{\int_{E_{\mathrm{thres}}}^{E_{\mathrm{max}}} \phi(E)\, dE}$ and $\bar{\sigma} = \frac{\int_{E_{\mathrm{thres}}}^{E_{\mathrm{max}}} \phi(E)\sigma(E) dE}{\int_{E_{\mathrm{thres}}}^{E_{\mathrm{max}}} \phi(E) dE}$ are the average energy of the neutron flux on the plutonium sample and the average ($n$, 2$n$) cross section, respectively; $E_{\mathrm{thres}} = 5.67$ MeV is the neutron energy threshold of the $^{239}$Pu($n$, 2$n$) $^{238}$Pu reaction and $\overline{\phi} = \int_{E_{\mathrm{thres}}}^{E_{\mathrm{max}}} \phi(E) dE$ is the average fluence determined per source neutron by the MCNP calculation.

The irradiation parameters for both measurements are summarized in Table V.

Error bars according to the data points in Fig. 18 account only for the statistical uncertainties. Because the $^{239}$Pu($n$, 2$n$) $^{238}$Pu cross section varies linearly with neutron energy over the energy spread range of the neutron beam on the plutonium deposits, the $x$-axis uncertainties do not include the neutron energy spread. In other words, the cross section at the average neutron energy is a very good approximation of the average cross section. From the ten measured cross sections, an average cross section can be extracted (black triangle and red line in Fig. 18). The obtained values with their uncertainties are given in Table VI. These uncertainties account for the counting statistics of the measurements and for the systematic errors. The systematics errors are composed of the uncertainties of McNabb *et al.* [10] propagated to lower-energy data points, the collection efficiency uncertainty, and that of the neutron standard monitors. The uncertainty of this data point, which considers the uncertainty generated by the interpolation process, has been propagated to the lower-energy data points.

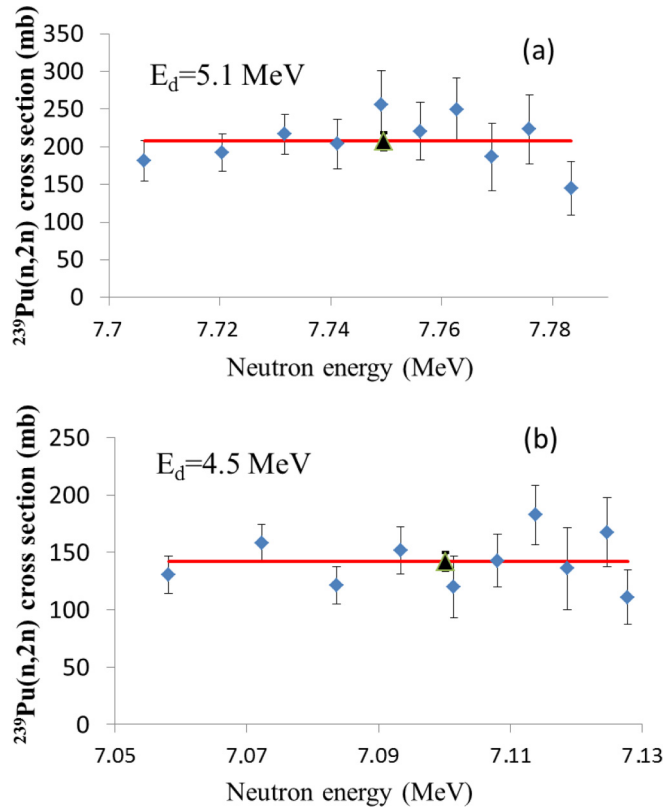


FIG. 18. $^{239}$Pu($n$, 2$n$) $^{238}$Pu cross section for each deposit. (a) For $E_d = 5.08$ MeV and (b) for $E_d = 4.47$ MeV. The black triangles and red lines are the average cross sections.

## VI. RESULTS AND DISCUSSION

Measurements of the $^{239}$Pu($n$, 2$n$) $^{238}$Pu cross section obtained with the recoil technics are shown in Fig. 19 (black squares). Present experimental values have been assigned under the assumption that the collection efficiency does not vary between 9.3 and 7 MeV, which was confirmed by the $^{238}$U($n$, 2$n$) $^{237}$U measurement. The final uncertainties are dominated by the systematic uncertainty arising from the data of Becker *et al.* [8] that was adopted as a reference to normalize our data at 9.3 MeV.

Clearly, our data at 7.1 and 7.7 MeV are compatible with those of Becker *et al.* [8] and with the ENDF/BVIII.0 evaluated

TABLE VI. $^{239}$Pu($n$, 2$n$) cross sections and error bars obtained in this paper using the linear interpolation of the data of Becker *et al.* [8] at 9.34 MeV as a reference.

| Neutron energy (MeV) | $\sigma_{n2n}$ (mb) | Error (mb) | Statistical errors (mb) | Systematic errors (mb) |
|---|---|---|---|---|
| 7.10 | 142.0 | 23.3 | 7.7 | 22.0 |
| 7.72 | 207.3 | 34.0 | 10.4 | 32.4 |
| 9.34 | 269.0 | 40.3 | | 40.3 |

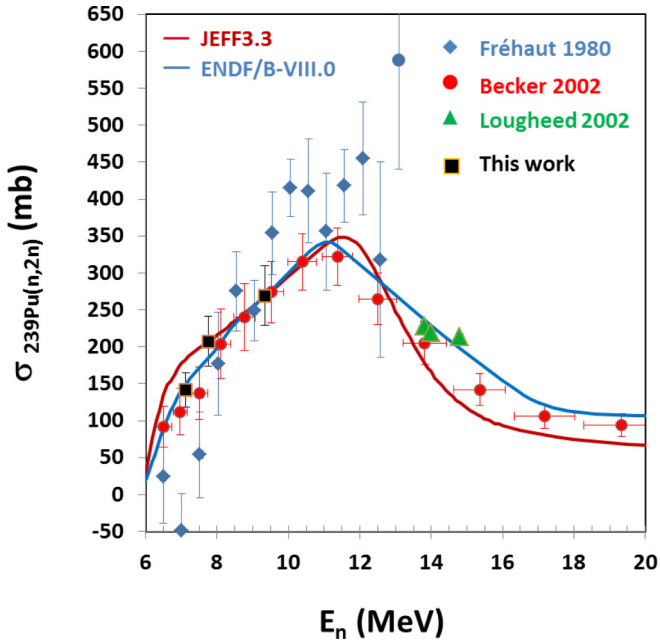


FIG. 19. Comparison of the experimental $^{239}$Pu$(n, 2n)$ $^{238}$Pu cross-section values obtained using the recoil method compared with previous experimental data and with the JEFF3.3 and ENDF/B-VIII.0 evaluations. The point at 9.3 MeV is normalized to existing data and evaluations. The points at 7.1 and 7.7 MeV are relative to the point at 9.3 MeV.

cross section. We, thus, confirm the lowering of the cross section for $E_n < 7.7$ MeV observed by Becker *et al.* [8] and Fréhaut *et al.* [6], a magnitude that cannot be reproduced by JEFF3.3. Although the JEFF3.3 value at 7.7 MeV remains consistent with our measurement, the difference between the cross section evaluated at 7.1 MeV and our measurement is beyond 1.8 standard deviation. A similar behavior for the $(n, 2n)$ cross section just above the energy threshold is observed for the $^{235}$U$(n, 2n)$ $^{234}$U reaction [32].

## VII. CONCLUSION

The cross sections for $^{239}$Pu$(n, 2n)$ $^{238}$Pu have been measured at 7.1 MeV, slightly above the reaction threshold and at 7.7 MeV by using the recoil method for counting the $^{238}$Pu nuclei. Our measured values are given normalized to the previously published data of Becker and co-workers [8,9] performed at 9.3 MeV, and their associated uncertainties are below 10%. The present paper confirms without ambiguity the disagreement observed between the previously published measurements and the JEFF3.3 evaluation in the region of the $^{239}$Pu$(n, 2n)$ reaction threshold.

In the frame of our study of the $^{239}$Pu$(n, 2n)$ $^{238}$Pu reaction, a new experiment is planned in the near future to measure $(n, 2n)$ cross sections at neutron energies between 9 and 20 MeV by using the *neutron for science* (NFS) neutron source [36] located at the GANIL facility (Caen, France). This experiment will use a high efficiency $4\pi$ neutron counter coupled to a veto fission chamber [37] to discriminate fission events. The high neutron flux of the NFS source associated with this detector should allow to produce a set of model-independent data, which could be used to normalize the present data.

## ACKNOWLEDGMENTS

We would like to thank all the technical staff at the facilities of CEA/DAM Ile de France, whose contributions made this work possible. We are especially thankful to the staff of the 7 MV Tandem for their strong involvement in this experience.

[1] P. Chudoba, A. Krása, J. Vrzalová, O. Svoboda, S. Kilim, V. Wagner, M. Majerle, M. Štefánik, M. Suchopár, A. Kugler *et al.*, Nucl. Sci. Eng. **191**, 150 (2018).

[2] M. Yuly,T. Eckert, G. Hartshaw, S. J. Padalino, D. N. Polsin, M. Russ, A. T. Simone, C. R. Brune, T. N. Massey, C. E. Parker *et al.*, Phys. Rev C **97**, 024613 (2018).

[3] OECD-NEA report Spent Nuclear Fuel Assay Data for Isotopic Validation NEA/NSC/WPNCS/DOC(2011)5, 2011 (unpublished).

[4] G. Deissmann, S. Neumeier, G. Modolo, and D. Bosbach, Review of the durability of potential plutonium wasteforms under conditions relevant to geological disposal, Forschungszentrum Jülich and Brenk Systemplanung Report, 2011 (unpublished).

[5] C. H. M. Broeders and G. Kessler, Nucl. Sci. Eng. **156**, 1 (2007).

[6] J. Fréhaut, A. Bertin, B. Bois, E. Gryntakis, and C. A. Phlis, Radiat. Eff. **96**, 219 (1986).

[7] R. W. Lougheed, W. Webster, M. N. Namboodiri, D. R. Nethaway, K. J. Moody, J. H. Landrum, R. W. Hoff, R. J. Dupzyk, J. H. Mcquaid, R. Gunnink *et al.*, Radio Acta **90**, 833 (2002).

[8] J. A. Becker, L. A. Bernstein, W. Younes, D. P. McNabb, P. E. Garrett, D. E. Archer, C. A. McGrath, M. A. Stoyer, H. Chen, W. E. Ormand *et al.*, J. Nucl. Sci. Technol, Suppl. **39**, 620 (2002).

[9] L. A. Bernstein, J. A. Becker, P. E. Garrett, W. Younes, D. P. McNabb, D. E. Archer, C. A. McGrath, H. Chen, W. E. Ormand, and M. A. Stoyer, Phys. Rev. C **65**, 021601(R) (2002).

[10] D. P. McNabb, J. D. Anderson, R. W. Bauer, J. A.Becker, F. Dietrich, P. Navratil, M. B. Chadwick, and P. G. Young, Evaluation of the $^{239}$Pu$(n, 2n)$ integrated cross section, Lawrence Livermore National Laboratory Report No. UCRL-ID-143328, 2001 (unpublished).

[11] P. G. Young, E. D. Arthur, and M. B. Chadwick, Comprehensive Nuclear Model Calculations: Theory and Use of the GNASH code, Proceedings of the workshop on nuclear reaction data and nuclear reactors, edited by A. Gandini and G. Reffo (ICTP, Trieste(Italy), 1996).

[12] A. Ross, H. Chen, G. Reffo, and R. M. White, The $^{239}$Pu$(n, 2n)$ $^{238}$Pu cross section: Preliminary Calculations (Lawrence Livermore National Laboratory, Report No. UCRL-ID-133497, 1999 (unpublished).

[13] M. Dupuis, S. Hilaire, S. Péru, E. Bauge, M. Kerveno, P. Dessagne, and G. Henning, EPJ Web Conf. **146**, 12002 (2017).
[14] J.-P. Jeukenne, A. Lejeune, and C. Mahaux, Phys. Rev. C **16**, 80 (1977).
[15] M. Dupuis, E. Bauge, S. Hilaire, F. Lechaftois, S. Péru, N. Pillet, and C. Robin, Eur. Phys. J. A **51**, 168 (2015).
[16] S. Péru, G. Gosselin, M. Martini, M. Dupuis, S. Hilaire, and J.-C. Devaux, Phys. Rev. C **83**, 014314 (2011).
[17] P. Romain, B. Morillon, and H. Duarte, Nucl. Data Sheets **131**, 222 (2016).
[18] E. Bauge, G. Bélier, J. Cartier, A. Chatillon, J. M. Daugas, J. P. Delaroche, P. Dossantos-Uzarralde, H. Duarte, N. Dubray, M. Ducauze-Philippe *et al.*, Eur. Phys. J. A **48**, 113 (2012).
[19] A. J. M. Plompen, O. Cabellos, C. De Saint Jean, M. Fleming, A. Algora, M. Angelone, P. Archier, E. Bauge, O. Bersillon, A. Blokhin *et al.*, Eur. Phys. J. A **56**, 181 (2020).
[20] D. A. Brown, M. B. Chadwick, R. Capote, A. C. Kahler, M. W. Herman A.Trkov, A. A. Sonzogni, Y. Danon, A. D. Carlson, M. Dunn *et al.*, Nucl. Data Sheets **148**, 1 (2018).
[21] J. Tommasi, and G. Noguere, Nucl. Sci. Eng. **160**, 232 (2008).
[22] B. Laurent, V. Méot, and O. Roig, Development of a deuterium target for neutrons production at the CEA-DAM Ile de France tandem facility (unpublished).
[23] A. Ghiorso, B. G. Harvey, G. R. Choppin, S. G. Thompson, and G. T. Seaborg, Phys. Rev. **98**, 1518 (1955).
[24] M. Götz, S. Götz, J. V. Kratz, C. E. Düllmann, C. Mokry, J. Runke, P. Thörle-Pospiech, N. Wiehl, M. Schädel, J. Ballof *et al.*, Nucl. Phys. A **961**, 1 (2017).
[25] J. D. Hemingway, R. H. James, E. B. Martin, and G. R Marin, Proc. R. Soc. London, Series A **292**, 180 (1966).
[26] A. Yamadera, Y. Uno, and T. Nakamura, Nucl. Instrum. Methods Phys. Res., Sect. A **329**, 188 (1993).
[27] V. R. Sharma, A. Yadav, P. P. Singh, D. P. Singh, Unnati, R. Kumar, B. P. Singh, R. Prasad, and A. K. Sinha, EPJ Web Conf. **17**, 16012 (2011).
[28] V. Métivier, C. Duchemin, A. Guertin, N. Michel, and F. Haddad, EPJ Web Conf. **146**, 04058 (2017).
[29] J. F. Ziegler, J. P. Biersack, and M. D. Ziegler, SRIM, *The Stopping and Range of Ions in Matter* (Lulu, Morrisvile, 2009), [http://www.srim.org]
[30] ENSDF: https://www.nndc.bnl.gov/ensdf/
[31] M. Mayer, SIMNRA User's Guide, Report No. IPP 9/113, *Max-Planck-Institut für Plasmaphysik*, Garching, Germany, 1997 (unpublished).
[32] EXFOR : https://www.nndc.bnl.gov/exfor/
[33] X-5 Monte Carlo Team MCNP, Version 5 Overview and Theory Report No. LA-UR-03-1987, Vol. I, 2003 (unpublished).
[34] A. Cagniant, O. Delaune, M. Réglat, G. Douysset, P. Gross, and G. Le Petit, Appl. Radiat. and Isot. **126**, 197 (2017).
[35] E. Birgersson, and G. Lovestam, JRC Science Hub Technical Report No. 23794, 2009 (unpublished).
[36] X. Ledoux, M. Aıche, M. Avrigeanu, V. Avrigeanu, E. Balanzat, B. Ban-d'Etat, G. Ban, E. Bauge, G. Belier, P. Bem *et al.*, EPJ Web Conf. **146**, 03003 (2017).
[37] G. Bélier (private communication).